ICCFD13-2026-365

Shock Speed Deviations Induced by Non-Conservative Effects in One-Dimensional Conservation Laws

R.Guglielmi*, A.Rausa*, B.Re* and A. Guardone*
Corresponding author: riccardo.guglielmi@polimi.it
* Department of Aerospace Science and Technology, Politecnico di Milano, Italy.

Abstract: Non-conservative numerical operations may alter the propagation of discontinuities in hyperbolic conservation laws by violating the integral balances underlying the Rankine-Hugoniot conditions. Among the various sources of non-conservativity encountered in computational fluid dynamics, mesh-transfer procedures are particularly relevant in moving-mesh, adaptive, and re-meshing frameworks, where the numerical solution must be repeatedly projected between different computational grids. In this work, the effect of non-conservative mesh-transfer operations on shock propagation is investigated. A theoretical framework is developed to relate the conservation defects introduced during the remapping process to deviations in shock speed. For a nearest-neighbour transfer operator, it is shown that the artificial displacement of a discontinuity generates spurious conserved quantities that can be interpreted as localized source terms attached to the shock. The analysis is first derived for Burgers' equation and subsequently extended to the Euler system in terms of mass, momentum, and energy conservation defects. The theoretical predictions are assessed through a series of finite-volume simulations on moving meshes. In all test cases considered, the shock-speed deviations observed in the non-conservative solutions are accurately predicted from the conservation defects introduced by the remapping procedure. The results demonstrate that incorrect shock propagation is a direct consequence of non-conservation and provide a quantitative framework for predicting shock-speed errors in the presence of non-conservative numerical operations.

Keywords: Shock Wave Propagation, Non-Conservative Effects, ALE Formulation, Mesh Transfer.

1. Introduction

Shock waves are a fundamental feature of nonlinear hyperbolic conservation laws and may emerge spontaneously from smooth initial data through wave steepening. In compressible CFD, their accurate resolution is essential, since even small errors in shock speed or position may accumulate over time and significantly degrade the accuracy of the numerical solution. For systems of conservation laws, the propagation speed of discontinuities is uniquely determined by the Rankine–Hugoniot jump conditions, which follow directly from the integral conservation principle. As a consequence, preserving conservation at the discrete level is essential for obtaining physically correct shock dynamics. This requirement forms the basis of conservative finite-volume methods, widely used for the simulation of compressible flows and related nonlinear problems [1].

In practical CFD applications, however, strict conservation may be violated for several reasons. For example, in several contexts, it may be advantageous to reformulate the governing equations in non-conservative or primitive-variable form. Such approaches are often motivated by their more direct access to physically meaningful variables, their potential to simplify the numerical treatment of complex physical models, their improved conditioning in low-Mach-number regimes [2], and their ability to facilitate the enforcement of positivity-preserving properties [3]. However, unless special corrective measures are employed, discretizations based on non-conservative variables do not generally guarantee the exact preservation of the conserved quantities at the discrete level. Conservation errors may also arise even when the underlying discretization is formulated in conservative form. A particularly important example occurs when the numerical solution is transferred between different computational meshes. Such transfers arise naturally in adaptive mesh refinement, dynamic mesh adaptation, moving-mesh methods, re-meshing procedures, overset-grid approaches, and multi-physics simulations involving non-matching discretizations. The transfer of solution data between meshes is commonly performed through interpolation or projection operators, whose primary objective is often the preservation of local accuracy. Unless specifically designed to do so, however, these operators do not necessarily preserve the globally conserved quantities of the governing equations. Conservative remapping techniques have therefore been developed to guarantee exact preservation of mass, momentum, and energy across mesh changes [4]. An alternative strategy consists of performing a non-conservative transfer followed by a corrective repair step designed to restore the conservation of the transferred quantities [5]. This additional repair stage, however, comes at the price of increased computational effort. As a consequence, simpler non-conservative approaches remain attractive because of their algorithmic simplicity and low computational cost.

The present work investigates the relationship between conservation errors generated during mesh transfer and the resulting deviations in shock speed. To isolate and quantify this mechanism, we consider one-dimensional Riemann problems for both the inviscid Burgers' equation and the compressible Euler equations. The Burgers' equation provides a simple scalar framework in which the connection between conservation errors and shock motion can be analyzed transparently, while the Euler equations demonstrate the relevance of the phenomenon for realistic compressible-flow systems. Numerical experiments are performed by comparing a fully conservative reference solution with a solution subjected to repeated non-conservative mesh-transfer operations, thereby systematically altering shock propagation through the introduction of spurious conserved quantities. The present paper is structured as follows. Section 2 presents the theoretical framework developed to relate conservation defects introduced by non-conservative mesh-transfer operations to shock-speed errors. The analysis is first carried out for the inviscid Burgers' equation and subsequently extended to the one-dimensional Euler equations. Section 3 presents the corresponding numerical validation for both test cases. Finally, Section 4 summarizes the main findings and discusses possible directions for future research.

2. Methodology

Since mesh-transfer operations only arise when the computational mesh changes in time, the numerical framework considered in this work is based on a finite-volume discretization on a moving grid. Two different strategies are employed to account for the mesh motion. The first is a fully Arbitrary Lagrangian-Eulerian (ALE) formulation, in which the mesh velocity is directly incorporated into the numerical flux function. In this framework, the solution remains associated with the same control volumes throughout the simulation and conservation is preserved by construction. As a result, no transfer of the solution between different meshes is required. The second strategy adopts an Eulerian formulation, in which the governing equations are solved on a sequence of different meshes. At each time step, the solution computed on the old mesh must therefore be projected onto the new mesh through a mesh-transfer procedure. Unlike the ALE formulation, the conservation properties of the overall method are no longer determined solely by the finite-volume discretization, but also depend on the transfer operator employed to reconstruct the solution on the updated mesh. The conceptual difference between the two approaches is illustrated in Figure 1. In the ALE framework, the numerical solution remains attached to the moving mesh, and its evolution is entirely determined by the conservative finite-volume update. In the Eulerian framework, the numerical solution is first advanced on the old mesh and subsequently transferred onto the new mesh.

Among the many transfer operators available in the literature, the nearest-neighbour (NN) procedure is considered in the present work because of its simplicity and robustness. The method consists of assigning to each target cell the solution value associated with the closest cell of the source mesh. In a formula,

$$u_j^{n+1} = u_{i^\star}^n \qquad i^* = \arg\min_i \left| x_j^{n+1} - x_i^n \right| . \tag{1}$$

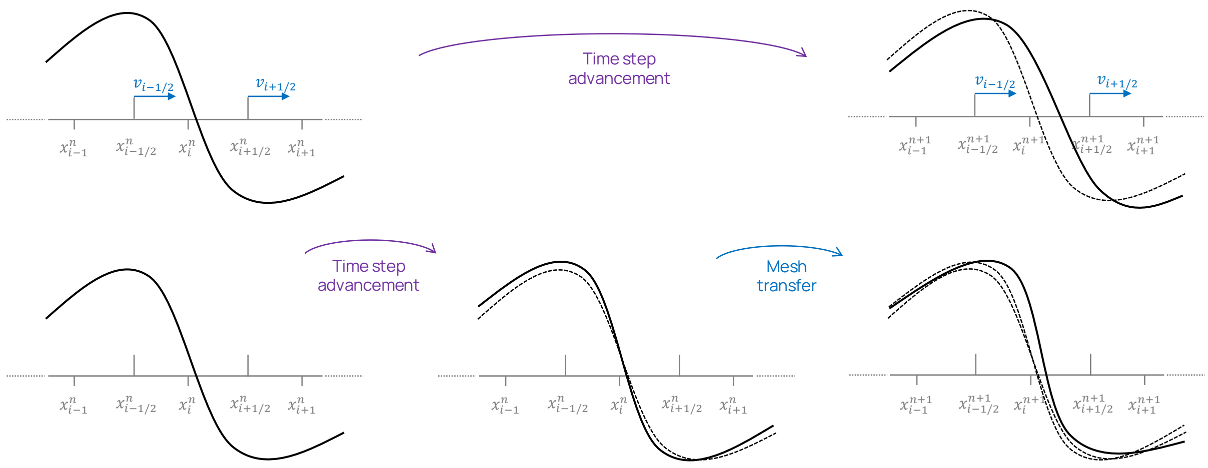

Figure 1: Comparison between the fully ALE formulation and the Eulerian formulation followed by a mesh-transfer step.

The NN operator is formally first-order accurate. Furthermore, because each target value is directly copied from an existing source value, no new extrema can be generated during the transfer process. The method is therefore monotone and preserves the range of the numerical solution. These properties make it particularly attractive in the presence of strong discontinuities. Despite these advantages, the NN interpolation is generally not conservative. The total amount of conserved quantities after the transfer does not necessarily coincide with that of the original mesh, and spurious mass, momentum, or energy may be introduced into the computational domain. In the following subsections, we investigate how the conservation defects introduced by NN transfer affect shock propagation by considering Riemann problems for the inviscid Burgers' equation and the compressible Euler equations.

2.1 Inviscid Burgers' equation

The inviscid Burgers' equation reads

$$\frac{\partial u}{\partial t} + \frac{\partial\left[f(u)\right]}{\partial x} = 0\ , \ f(u) = \frac{u^2}{2}\ , \tag{2}$$

where $x \in [0, L], t \in [0, T]$. Providing as initial conditions piecewise constant data

$$u(x,0) = \begin{cases} u_L & x < x_0 \\ u_R & x > x_0 \end{cases}\ , \tag{3}$$

with $u_L > u_R$, the exact solution consists of a single shock propagating at a speed which follows the Rankine–Hugoniot condition

$$V_s = \frac{f(u_L) - f(u_R)}{u_L - u_R} = \frac{u_L + u_R}{2}\ . \tag{4}$$

For the analysis that follows, it is convenient to introduce the numerical mass, defined as the integral of the solution over the computational domain,

$$M(t) = \int_0^L u(x,t)\ dx\ . \tag{5}$$

For the piecewise-constant shock solution, the numerical mass can be expressed as

$$M = u_L x_s + u_R(L - x_s)\ , \tag{6}$$

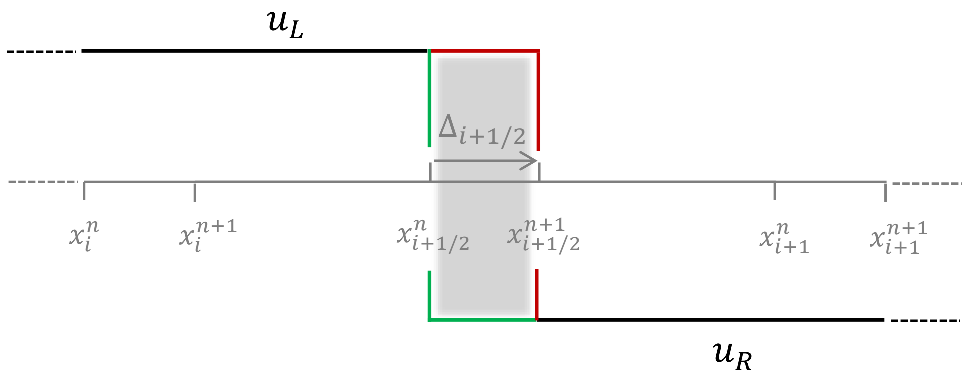

Figure 2: Shock displacement induced by a NN mesh transfer. The shaded region represents the conservation defect introduced during the transfer.

where x_s denotes the shock position and time dependence has been omitted for brevity. The previous expression highlights the direct relationship between the mass contained in the domain and the location of the discontinuity. Differentiating equation (6) with respect to time yields

$$\frac{dM}{dt} = (u_L - u_R)V_s \ , \tag{7}$$

showing the explicit relation between shock speed and the time derivative of the numerical mass.

To isolate the effect of the mesh-transfer procedure, we assume that the finite-volume solution is represented through a piecewise-constant reconstruction and that the discontinuity is exactly aligned with a cell interface. At time t^n, the shock is located at the interface $x^n_{i+1/2}$, separating the constant states u_L and u_R. After the mesh motion, the same interface is displaced to $x^{n+1}_{i+1/2}$. When an NN transfer is employed, the cell values are copied onto the nearest cells of the new mesh. The discontinuity is therefore reassigned to a different interface location and becomes effectively dragged by the mesh motion, independently of the physical propagation prescribed by the Rankine-Hugoniot condition. The process is illustrated in Figure 2. Denoting by $\Delta_{i+1/2}$ the displacement of the interface due to mesh motion, since the left and right states remain unchanged, the only effect of the remapping is the modification of the region occupied by each constant state. As shown in Figure 2, this produces a spurious variation of mass equal to the area swept by the displaced discontinuity,

$$\Delta M = \Delta_{i+1/2}(u_L - u_R). \tag{8}$$

The numerical mass associated with the non-conservative transfer can therefore be written as

$$M^{NC} = M^C + \Delta M, \tag{9}$$

where M^C denotes the mass obtained through a conservative update. Using equation (9), the relation between the conservative and non-conservative shock speeds is

$$V_s^{NC} = V_s^C + \frac{1}{u_L - u_R}\left(\frac{dM^{NC}}{dt} - \frac{dM^C}{dt}\right) = V_s^C + \frac{1}{u_L - u_R}\frac{d\Delta M}{dt} \ . \tag{10}$$

Equation (10) establishes a direct connection between the conservation defect introduced during the remapping step and the resulting deviation of the shock speed from its conservative counterpart. The additional term may be interpreted as a shock-attached source of mass, whose strength is equal to the rate at which mass is artificially introduced by the non-conservative transfer. Therefore, a non-conservative mesh-transfer operation does not merely perturb the solution locally, but directly modifies the propagation law of the discontinuity through the violation of the underlying conservation principle. In the particular case considered here, the conservation defect originates from the displacement of the mesh interface.

Differentiating equation (8) with respect to time yields

$$\frac{d\Delta M}{dt} = (u_L - u_R) v_{i+1/2}, \tag{11}$$

where $v_{i+1/2}$ denotes the velocity of the interface carrying the discontinuity. Substituting into equation (10) immediately gives

$$V_s^{NC} = V_s^C + v_{i+1/2}, \tag{12}$$

showing that the mesh motion contributes directly to the propagation speed of the discontinuity. Nevertheless, this result is specific to the present configuration and relies on the explicit knowledge of the interface displacement and velocity. By contrast, equation (10) is independent of the specific transfer operator and remains valid whenever the remapping procedure introduces a conservation defect while leaving the states connected by the discontinuity unchanged. Its practical advantage is that it relates the shock-speed deviation directly to the evolution of the conserved quantities, which can be readily evaluated from the numerical solution without requiring any information about the local mesh motion. Consequently, equation (10) provides a general framework for quantifying shock-speed errors induced by non-conservative transfer procedures.

2.2 Euler equations

The Euler system of equations, written in terms of the conservative variables density ρ, momentum $m = \rho u$, and total energy $E = \rho(e + \frac{1}{2}\rho u^2)$, reads

$$\frac{\partial \boldsymbol{U}}{\partial t} + \frac{\partial \left[\boldsymbol{F}(\boldsymbol{U})\right]}{\partial x} = 0\ ,\ \boldsymbol{U} = \begin{bmatrix} \rho \\ m \\ E \end{bmatrix}\ ,\ \boldsymbol{F}(\boldsymbol{U}) = \begin{bmatrix} m \\ \frac{m^2}{\rho} + p \\ (E+p)\frac{m}{\rho} \end{bmatrix} = \begin{bmatrix} m \\ \frac{1}{2}(3-\gamma)\frac{m^2}{\rho} + (\gamma-1)E \\ -\frac{1}{2}(\gamma-1)\frac{m^3}{\rho^2} + \gamma\frac{mE}{\rho} \end{bmatrix}\ , \tag{13}$$

where $x \in [0, L], t \in [0, T]$ and under ideal gas law assumption the pressure is given by $p = (\gamma - 1)(E - \frac{1}{2}\frac{m^2}{\rho})$, with $\gamma = 1.4$. Providing as initial conditions piecewise constant data

$$\boldsymbol{U}(x,0) = \begin{cases} \boldsymbol{U}_L = [\rho_L\ m_L\ E_L]^T & x < x_0 \\ \boldsymbol{U}_R = [\rho_R\ m_R\ E_R]^T & x > x_0 \end{cases}\ , \tag{14}$$

with $u_L > u_R$, the exact solution consists of three elementary waves: a shock wave, a contact discontinuity, and a rarefaction fan. These features are separated by regions in which the conservative variables remain constant. Different from Burgers' equation, the Euler system contains three conservation laws associated with the conserved variables density, momentum, and total energy. It is therefore natural to introduce the corresponding integral quantities

$$\begin{cases} M_\rho = \int_0^L \rho(x,t)\ dx \\ M_m = \int_0^L m(x,t)\ dx \\ M_E = \int_0^L E(x,t)\ dx \end{cases} \tag{15}$$

representing the total mass, momentum, and energy contained in the computational domain.

In order to isolate the effect of the mesh-transfer procedure on the shock propagation, the mesh motion is restricted to a region surrounding the shock wave, while the contact discontinuity and the rarefaction fan remain unaffected by the remapping process. Under this assumption, the conservation defects introduced by the transfer originate exclusively from the displacement of the shock interface, allowing the same geometrical arguments developed for Burgers' equation to be applied. Let $\Delta_{i+1/2}$ denote again the displacement of the shock interface induced by the mesh motion, as in Figure 2. Since the conservative variables remain piecewise constant on either side of the discontinuity, the NN transfer modifies the amount of conserved quantities contained in the domain by an amount proportional to the shock displacement. The resulting conservation defects are

$$\begin{cases} \Delta M_\rho = \Delta_{i+1/2}\left(\rho_L - \rho_R\right) \\ \Delta M_m = \Delta_{i+1/2}\left(m_L - m_R\right) \\ \Delta M_E = \Delta_{i+1/2}\left(E_L - E_R\right) \end{cases} \tag{16}$$

where the left and right states refer, as usual, to the states immediately adjacent to the shock. The numerical solutions obtained through conservative and non-conservative transfers, therefore, satisfy

$$\begin{cases} M_\rho^{NC} = M_\rho^C + \Delta M_\rho \\ M_m^{NC} = M_m^C + \Delta M_m \\ M_E^{NC} = M_E^C + \Delta M_E \end{cases} \tag{17}$$

Proceeding exactly as in the Burgers case, the shock-speed deviation can be related to the conservation defects through

$$\begin{cases} V_s^{NC} = V_s^C + \frac{1}{\rho_L - \rho_R}\left(\frac{dM_\rho^{NC}}{dt} - \frac{dM_\rho^C}{dt}\right) = V_s^C + \frac{1}{\rho_L - \rho_R}\frac{d\Delta M_\rho}{dt} \\ V_s^{NC} = V_s^C + \frac{1}{m_L - m_R}\left(\frac{dM_m^{NC}}{dt} - \frac{dM_m^C}{dt}\right) = V_s^C + \frac{1}{m_L - m_R}\frac{d\Delta M_m}{dt} \\ V_s^{NC} = V_s^C + \frac{1}{E_L - E_R}\left(\frac{dM_E^{NC}}{dt} - \frac{dM_E^C}{dt}\right) = V_s^C + \frac{1}{E_L - E_R}\frac{d\Delta M_E}{dt} \end{cases} \tag{18}$$

These expressions establish a direct connection between the shock-speed error and the rates at which mass, momentum, and energy are artificially introduced by the non-conservative transfer. Therefore, similarly to the Burgers equation, the effect of the remapping procedure can be interpreted as the action of localized sources of mass, momentum, and energy attached to the shock wave. It should be noted that the present configuration represents a particular case in which the conservation defects in mass, momentum, and energy all originate from the same shock displacement induced by the mesh motion. Consequently, the three localized source terms are not independent but are proportional to one another and produce a coherent modification of the shock propagation speed while leaving the states connected by the discontinuity unchanged. More generally, non-conservative numerical procedures may introduce independent defects in the conservation of mass, momentum, and energy. In such situations, the resulting source terms would no longer have the same intensity, and their effect would not be limited to a modification of the shock speed, but would also alter the left and right states adjacent to the discontinuity.

3. Results

The theoretical predictions derived in the previous section are now assessed through a series of numerical experiments involving both the Burgers' equation and the Euler system. The objective is to verify whether the shock-speed deviation induced by a non-conservative mesh-transfer operation can be accurately predicted from the evolution of the global conserved quantities. All simulations are performed using a cell-centered finite-volume discretization on a mesh composed of $n = 512$ control volumes. Numerical fluxes are computed using Roe's flux-difference splitting scheme [6], while time integration is performed with an explicit fourth-order Runge–Kutta method. Spatial reconstruction is carried out using the fifth-order Weighted Essentially Non-Oscillatory (WENO5) scheme [7], providing high-order accuracy in smooth regions while avoiding spurious oscillations near discontinuities.

The fully ALE formulation, for which exact satisfaction of the Geometric Conservation Law (GCL) is enforced [8], is used as the conservative reference solution. The non-conservative solution is obtained by applying a nearest-neighbour transfer after every time step, projecting the solution from the current mesh onto the corresponding ALE mesh. The shock location is identified through Harten's shock sensor [9], and the corresponding shock speed is obtained from the time derivative of the detected trajectory.

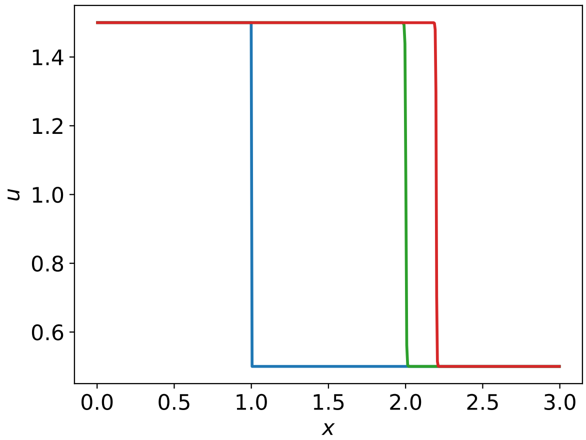

(a) Prescribed grid motion

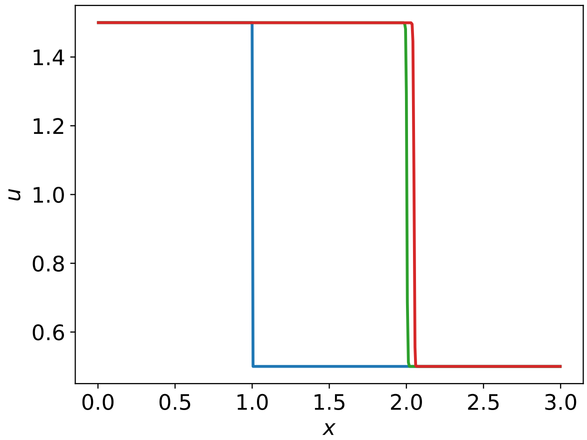

(b) Random grid motion

Figure 3: Comparison between conservative and non-conservative solution of inviscid Burgers' equation: — $u(x, 0)$, — $u^C(x, T)$, — $u^{NC}(x, T)$.

For each test case, four quantities are compared: the exact shock speed V_s^{EX}, the conservative shock speed V_s^C, the non-conservative shock speed V_s^{NC}, and the predicted non-conservative shock speed $\hat{V}_s^{NC}$ obtained from the theoretical relations derived in the previous section. Agreement between V_s^{NC} and $\hat{V}_s^{NC}$ would confirm that the shock-speed deviation is entirely determined by the conservation defects introduced during the remapping procedure.

3.1 Inviscid Burgers' equation

The Riemann problem is initialized with $u_L = 1.5$ and $u_R = 0.5$, yielding an exact shock speed $V_S^{EX} = 1$. The computational domain has length $L = 3$, and the simulation is advanced until $T = 1$ using a time step $\Delta t = 1.95 \times 10^{-4}$. Two different mesh motions are considered. In the first case, the shock propagates through a region where the mesh velocity is prescribed as a constant value $v = 0.2$, while the mesh remains stationary in the far left and far right portions of the domain. Although a constant mesh velocity is adopted for simplicity, the theoretical analysis developed in the previous section does not rely on this assumption and remains valid for spatially non-uniform and time-dependent grid velocity. In the second case, the shock propagates through a region where all cell interfaces undergo independent sinusoidal oscillations. The resulting cell size is

$$h_i(t) = \frac{L}{n} + \Delta_{i+1/2}(t) - \Delta_{i-1/2}(t) \ , \tag{19}$$

where

$$\Delta_k(t) = A_k \sin\left(\frac{2\pi t}{T_k} + \varphi_k\right) \ , \tag{20}$$

with

$$A_k \sim \mathcal{U}\left(-\frac{L}{2n}, \frac{L}{2n}\right), \qquad T_k \sim \mathcal{U}\,(0.003, 0.03) \ , \qquad \varphi_k \sim \mathcal{U}\,(0, 2\pi) \ , \tag{21}$$

where $\mathcal{U}(a, b)$ denotes the continuous uniform distribution in the interval $[a, b]$. The range of random amplitudes is selected so that no interface crossing occurs during the simulation, ensuring that all control volumes remain strictly positive. As in the previous case, the mesh remains stationary outside the region crossed by the shock.

Figure 3 compares the conservative and non-conservative solutions at the final time. In both mesh-motion scenarios, the left and right states remain unchanged, while the discontinuity undergoes a progressive displacement caused by the repeated NN transfers. Although the spurious numerical mass introduced by

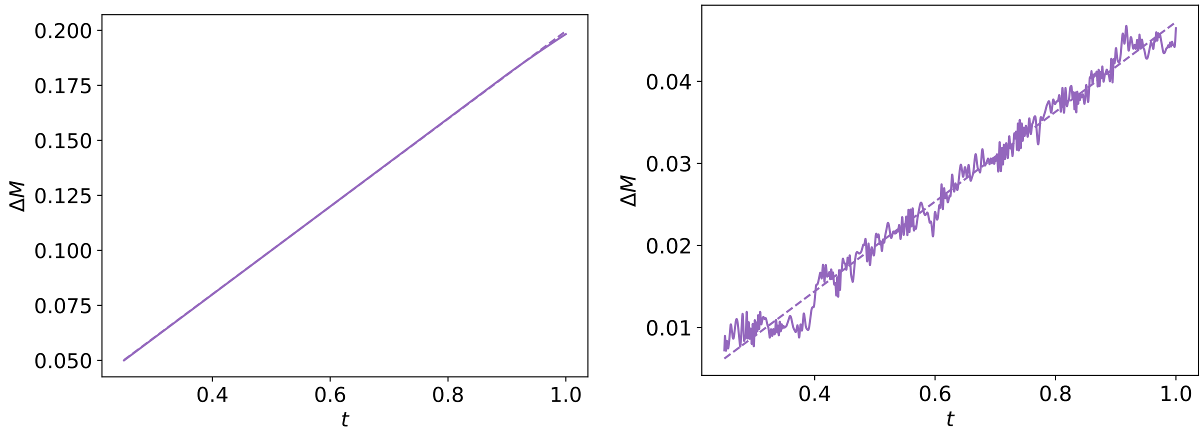

(a) Prescribed grid motion

(b) Random grid motion

Figure 4: Conservation defect generated by the NN transfer. The dashed line corresponds to the smoothed signal employed to evaluate its time derivative.

	Prescribed grid motion	Random grid motion
V_S^C	1.00001	0.99937
V_S^{NC}	1.20024	1.05425
$\hat{V}_S^{NC}$	1.19929	1.05469

Table 1: Comparison between the conservative shock speed V_s^C, the non-conservative shock speed V_s^{NC}, and the predicted non-conservative shock speed $\hat{V}_s^{NC}$ for the inviscid Burgers' equation.

each individual transfer is small, its cumulative effect leads to a significant displacement of the shock over the duration of the simulation. The conservation defects are reported in Figure 4. For the prescribed mesh motion, the mass imbalance grows linearly in time, reflecting the constant interface velocity. In contrast, the random mesh motion generates a highly oscillatory curve. In this case, a linear smoothing procedure is employed to estimate the mass derivative appearing in equation (10).

Finally, Table 1 summarizes the measured and predicted shock speeds. The conservative solution reproduces the exact shock speed with excellent accuracy, confirming that the ALE formulation preserves the correct propagation law. In the prescribed-velocity case, the non-conservative shock speed is approximately equal to the sum of the conservative shock speed and the imposed mesh velocity, in agreement with the analytical prediction derived in formula (12). More importantly, for both mesh motions, the predicted non-conservative shock speed $\hat{V}_s^{NC}$ is found to be in excellent agreement with the measured value V_s^{NC}. This result demonstrates that the shock-speed deviation is entirely explained by the conservation defect introduced during the remapping procedure. The small discrepancies observed in Table 1 are mainly due to the numerical differentiation required to estimate both the shock speed from Harten's sensor and the time derivative of the mass imbalance.

3.2 Euler equations

The Sod shock-tube problem [10] is adopted as a representative test case for the Euler equations. A diaphragm initially located at $x = 1.5$ separates a left state characterized by density $\rho_L = 1$, velocity $u_L = 0$, and pressure $p_L = 1$ from a right state with $\rho_R = 0.125$, velocity $u_R = 0$, and pressure $p_R = 0.1$. In terms of the conserved variables, the corresponding states are $m_L = 0$, $E_L = 2.5$, $m_R = 0$, and $E_R = 0.25$. Following the removal of the diaphragm, the solution evolves into the classical Riemann structure composed of a left-moving rarefaction fan, a contact discontinuity, and a right-moving shock

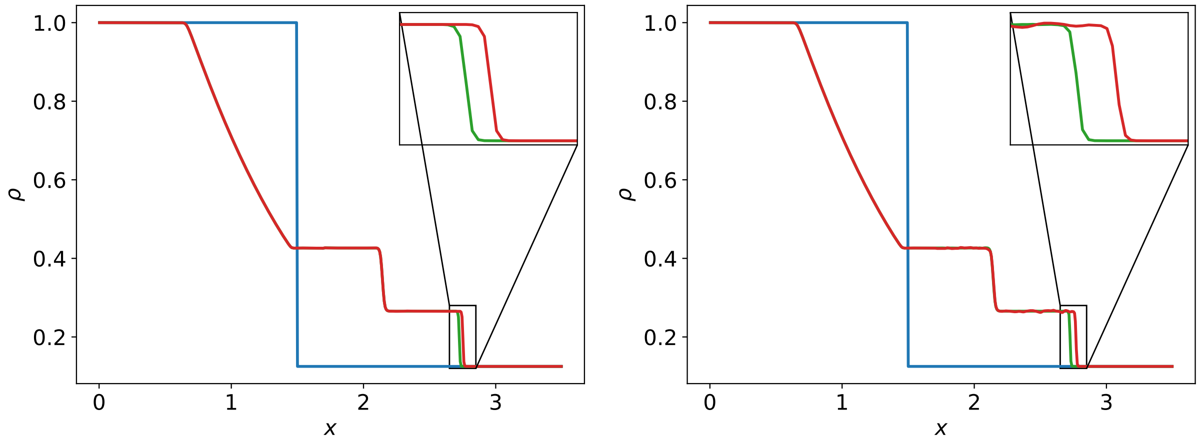

(a) Prescribed grid motion

(b) Random grid motion

Figure 5: Comparison between the conservative and non-conservative density fields for the Euler equations: — $\rho(x, 0)$, — $\rho^C(x, T)$, — $\rho^{NC}(x, T)$, with a zoom for $x \in [2.65, 2.85]$, $\rho \in [0.12, 0.28]$.

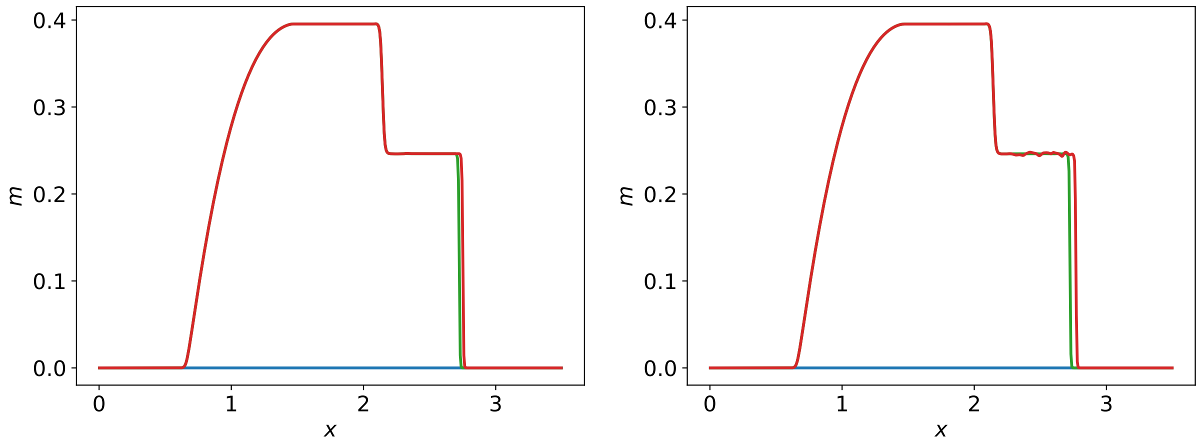

(a) Prescribed grid motion

(b) Random grid motion

Figure 6: Comparison between conservative and non-conservative momentum fields for the Euler equations: — $m(x, 0)$, — $m^C(x, T)$, — $m^{NC}(x, T)$.

wave. The exact shock speed is $V_s^{EX} = 1.75216$. Solid-wall boundary conditions are imposed at both ends of the domain. The computational domain has length $L = 3.5$, and the simulation is advanced until $T = 0.7$, before any wave reflection from the boundaries occurs, using a time step $\Delta t = 9.76 \times 10^{-5}$. As in the Burgers' test case, two different mesh motions are considered. In the first configuration, the mesh moves with a prescribed velocity $v = 0.05$. In the second configuration, the random mesh motion defined by equations (19), (20), (21) is employed. To isolate the effect of the transfer procedure on the shock dynamics, the mesh remains fixed in the regions crossed by the rarefaction fan and the contact discontinuity.

Figures 5, 6, and 7 compare the conservative and non-conservative solutions at the final simulation time for density, momentum, and total energy. Similar to the Burgers' equation, the repeated nearest-neighbour transfers induce a progressive displacement of the shock while leaving the states immediately adjacent to the discontinuity essentially unchanged. The resulting position error accumulates throughout the simulation despite the relatively small spurious global quantities introduced by each individual transfer operation. The conservation defects associated with mass, momentum, and total energy are reported in Figure 8. As observed for the Burgers' equation, the prescribed mesh motion generates a linear growth of

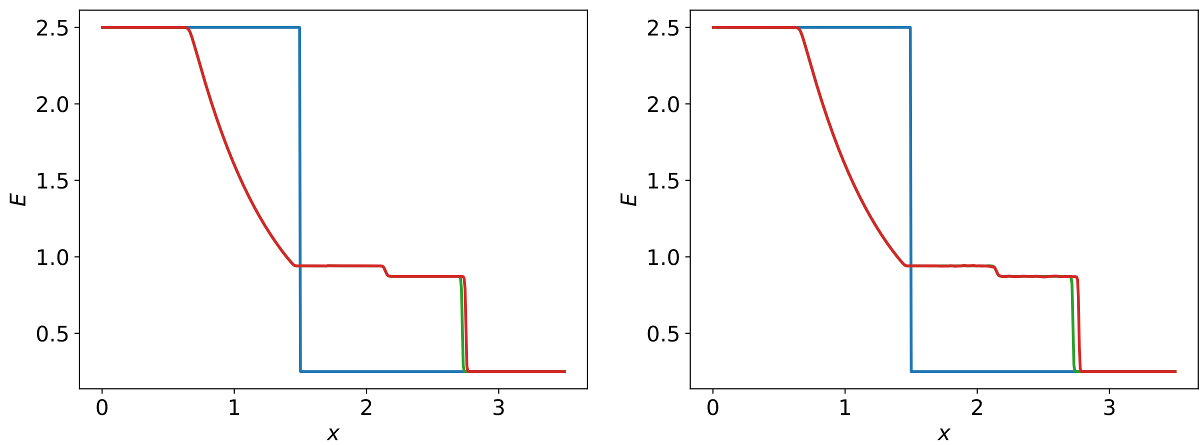

(a) Prescribed grid motion (b) Random grid motion

Figure 7: Comparison between conservative and non-conservative energy fields for the Euler equations: — $E(x,0)$, — $E^C(x,T)$, — $E^{NC}(x,T)$.

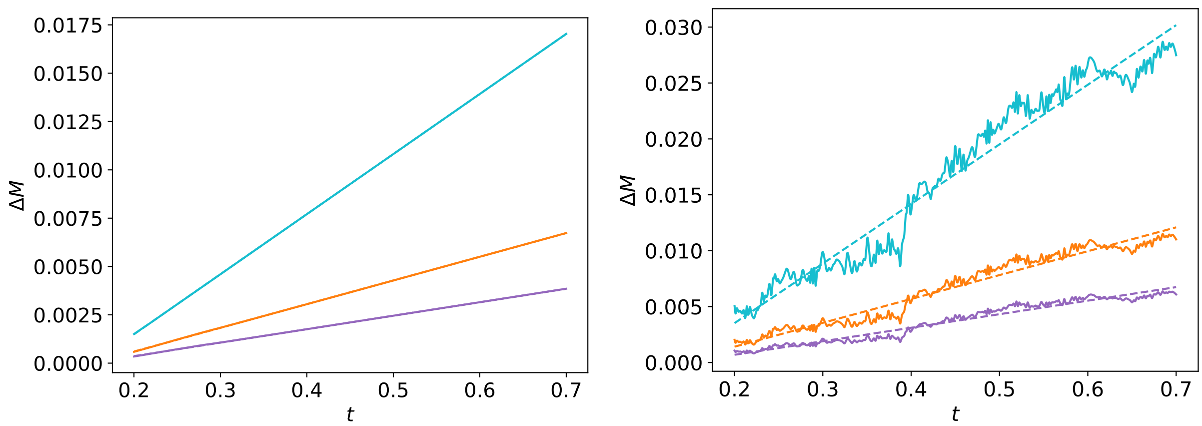

(a) Prescribed grid motion (b) Random grid motion

Figure 8: Conservation defects generated by the NN transfer: — ΔM_ρ, — ΔM_m, — ΔM_E. The dashed lines correspond to the smoothed signals employed to evaluate their time derivatives.

	Prescribed grid motion	Random grid motion
V_S^C	1.75204	1.75177
V_S^{NC}	1.80170	1.83391
$\hat{V}_S^{NC}$	1.80119	1.83826

Table 2: Comparison between the conservative shock speed V_s^C, the non-conservative shock speed V_s^{NC}, and the predicted non-conservative shock speed $\hat{V}_s^{NC}$ for the Euler equations.

the conservation error, whereas the random mesh motion produces strongly oscillatory defects. The latter are smoothed prior to evaluating the time derivatives appearing in the theoretical shock-speed prediction.

Shock-speed results are summarized in Table 2. To avoid contamination from the initial shock-formation transient, the reported values are computed using data for $t \geq 0.2$. Since the Euler system provides three independent estimates of the shock-speed correction based on mass, momentum, and energy conservation defects, the value reported for $\hat{V}_s^{NC}$ corresponds to the arithmetic average of the three predictions. The conservative solution reproduces the exact shock speed with excellent accuracy. In contrast, the NN transfer introduces a significant shock-speed deviation in both mesh-motion scenarios. Most importantly, the predicted non-conservative shock speed $\hat{V}_s^{NC}$ is found to be in excellent agreement with the value measured from the shock trajectory. This result demonstrates that the relationship established in the previous section is not limited to scalar conservation laws, but remains valid for the Euler equations despite the simultaneous presence of multiple conserved quantities and interacting wave families. It is worth noting that the prediction remains accurate even in the random mesh-motion case, for which no explicit relation analogous to $V_s^{NC} = V_s^C + v$ exists. This highlights the practical relevance of the conservation-defect formulation, which relies solely on the evolution of the global conserved quantities and therefore remains applicable to arbitrarily complex mesh motions.

4. Conclusions

This work investigated the effect of non-conservative mesh-transfer operations on the propagation of discontinuities in hyperbolic conservation laws. The attention was restricted to the nearest-neighbour transfer operator, which was employed as a simple and representative example of a non-conservative remapping procedure. A theoretical framework was developed to connect non-conservative remapping operations with shock-speed deviations. For the inviscid Burgers' equation, the artificial displacement of the discontinuity induced by the transfer was shown to generate a localized mass imbalance, resulting in a predictable modification of the shock propagation speed. The analysis was subsequently extended to the Euler equations, where analogous relations were derived in terms of the defects of the mass, momentum, and total energy in the domain.

The theoretical predictions were verified through a series of numerical experiments involving both prescribed and randomly moving meshes. In all cases considered, the shock-speed deviations observed in the non-conservative simulations were accurately predicted from the evolution of the global conserved quantities. The results demonstrate that the incorrect shock propagation induced by nearest-neighbour remapping is not merely a local interpolation error, but rather a direct consequence of the violation of the underlying conservation principle. These findings highlight the importance of conservation-preserving transfer procedures in adaptive, moving-mesh, and re-meshing simulations involving discontinuous solutions. More generally, they suggest that conservation defects provide a natural framework for interpreting and quantifying shock-speed errors arising from non-conservative numerical operations.

The present analysis also suggests several natural extensions. While the focus of this work has been on non-conservative mesh-transfer operations, similar mechanisms may arise from other sources of non-conservativity, such as discretizations formulated in primitive variables. Extending the proposed framework to these situations could provide a unified interpretation of shock-speed deviations originating from different numerical mechanisms. Furthermore, the nearest-neighbour operator considered here represents a particularly simple transfer procedure. Investigating how more sophisticated interpolation and projection operators influence wave propagation would help assess the generality of the present findings. In particular, the present study suggests that transfer operators preserving the conserved quantities exactly should not induce any systematic shock-speed deviation, since the mechanism identified here originates from the artificial introduction of mass, momentum, or energy during the remapping step. Finally, the analysis has been deliberately restricted to one-dimensional Riemann problems to isolate the underlying mechanism. An important next step is the application of the proposed framework to more realistic flow configurations, where multiple discontinuities interact, and the global imbalance introduced by the numerical procedure can no longer be associated with a single isolated shock wave.

References

[1] Randall J. LeVeque. *Numerical methods for conservation laws*, volume 132. Springer, 1992.

[2] Eli Turkel and Verr N Vatsa. Choice of variables and preconditioning for time dependent problems. In *16th AIAA CFD Conference*, 2003.

[3] Xiangxiong Zhang and Chi-Wang Shu. Maximum-principle-satisfying and positivity-preserving high-order schemes for conservation laws: survey and new developments. *Proceedings of the Royal Society A: Mathematical, Physical and Engineering Sciences*, 467(2134):2752–2776, 2011.

[4] LG Margolin and Mikhail Shashkov. Second-order sign-preserving conservative interpolation (remapping) on general grids. *Journal of Computational Physics*, 184(1):266–298, 2003.

[5] Raphaël Loubère, Martin Staley, and Burton Wendroff. The repair paradigm: New algorithms and applications to compressible flow. *Journal of Computational Physics*, 211(2):385–404, 2006.

[6] Philip L Roe. Approximate riemann solvers, parameter vectors, and difference schemes. *Journal of computational physics*, 43(2):357–372, 1981.

[7] Guang-Shan Jiang and Chi-Wang Shu. Efficient implementation of weighted ENO schemes. *Journal of computational physics*, 126(1):202–228, 1996.

[8] Paul Dennis Thomas and Charles K Lombard. Geometric conservation law and its application to flow computations on moving grids. *AIAA journal*, 17(10):1030–1037, 1979.

[9] Amiram Harten. The artificial compression method for computation of shocks and contact discontinuities. iii. self-adjusting hybrid schemes. *Mathematics of Computation*, 32(142):363–389, 1978.

[10] Gary A Sod. A survey of several finite difference methods for systems of nonlinear hyperbolic conservation laws. *Journal of computational physics*, 27(1):1–31, 1978.